Exploiting Spatio-Spectral Correlation for Impulse Denoising in Hyperspectral Images

Hemant Kumar Aggarwal*, Angshul Majumdar
{hemanta,angshul}@iiitd.ac.in

Indraprastha Institute of Information Technology-Delhi, India

Abstract

This paper proposes a technique for reducing impulse noise from corrupted hyperspectral images. We exploit the spatio-spectral correlation present in hyperspectral images to sparsify the datacube. Since impulse noise is sparse, denoising is framed as an L1-norm regularized L1-norm data fidelity minimization problem. We derive an efficient split Bregman based algorithm to solve the same. Experiments on real datasets show that our proposed technique yields better results than state-of-the-art denoising algorithms compared against.

keywords Impulse noise, Total variation, Split-Bregman

1 Introduction

Images captured at high spectral resolution mostly from ≈400 nm to 2500 nm range of electromagnetic spectrum are generally referred as hyperspectral images. These images generally have more than 100 spectral bands with very narrow spectral gaps. Owing to the narrow gaps, the images exhibit high spectral correlation. Random fluctuations in the power supply of satellite's sensor often corrupts these images by random valued impulse noise. Impulse noise can also arise when response of the sensor is saturated or when the sensor fails to sample. The fact that hyperspectral images are corrupted by impulse noise is relatively new [1, 2, 3]; all the references regarding impulse noise in hyperspectral images are from the last two years. Fig 1 shows an example image from Gulf dataset [4] having high valued impulse noise (white spots). Usually impulse noise is not the only kind of noise corrupting hyperspectral images, Gaussian noise is also present. However, Gaussian denoising is a widely addressed problem [1, 2]. But there have been no prior studies on impulse denoising from hyperspectral images. Therefore this problem of reducing impulse noise from hyperspectral images has been addressed in this work. There are two broad approaches to solve this problem. The first approach is to use median filtering and its variants [5, 6, 7, 8]. The other approach is to exploit the sparsity of the image in some transform domain and formulate denoising as an optimization problem.

Let x be original gray-scale image and y be noise corrupted image then impulse denoising problem can be expressed as ℓ_1-norm minimizing sparse recovery problem:

$$\min_z \ \|y - D^T z\|_1 + \lambda \|z\|_1, \tag{1}$$

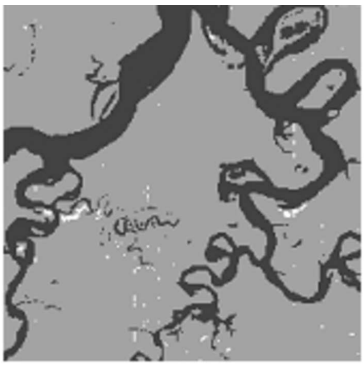

Figure 1: Band 180 of Gulf image. White spots corresponds to impulse noise.

where z is the sparse representation of image x in orthogonal sparsifying transform domain D such that $z = Dx$. This formulation is called the synthesis prior (SP) problem; here the sparse transform coefficients are recovered from which the image is synthesized. Here in Eq. (1) ℓ_1-norm of data fidelity term is minimized owing to the fact that impulse noise is sparse. Algorithms such as [9, 10, 11] have been proposed in past to solve this problem.

Another widely used approach for image denoising is total variation (TV) regularization[12] which can be represented as follows:

$$\|y - x\|_1 + \|D_h x\|_1 + \|D_v x\|_1, \tag{2}$$

where D_h, D_v are horizontal and vertical finite difference operators. Several algorithms such as [13, 14, 15, 16] have been proposed in literature to solve TV based impulse denoising problem. This formulation is referred to as analysis prior (AP) problem.

All these studies are restricted to single channel denoising; for our problem these methods have to be applied separately on each band of a hyperspectral image which does not account for inter-band correlation present in hyperspectral images.

Prior works in Gaussian noise removal from multi-band images have shown that exploiting the spectral correlation (along with spatial intra-band correlation) improves denoising performance. For example, there are TV based algorithms for color image denoising such as ColorTV[17], and MSBEL[18]. These algorithms are mainly designed for denoising of three channel color images. Algorithms have also been proposed for hyperspectral denoising based on spatial-spectral adaptive TV [1],spatial-spectral fusion technique [2] and spectral statis-

tics [19] based technique but these algorithms are designed for Gaussian noise reduction.

It has been shown previously in [20, 21] that exploiting spatio-spectral correlation leads to better reconstruction in compressive hyperspectral imaging. Following these studies we propose to exploit the inter-band spectral correlation and intra-band spatial correlation for denoising hyperspectral images corrupted by impulse noise. As the noise is sparse, we minimize ℓ_1-norm of data fidelity term. The spatio-spectral correlation leads to a sparse representation of the hyperspectral datacube in certain transform domains; the transform domain sparsity leads to ℓ_1-norm regularization of the ℓ_1-norm data fidelity. To the best of our knowledge there is no published work on denoising impulse noise corrupted hyperspectral images which utilizes both spatial redundancy and spectral correlation. We derive an efficient split-Bregman[22, 13] based algorithm to solve this problem.

In this work, we have explored two different models namely synthesis prior and analysis prior and experimentally found that synthesis prior model yields better results than analysis prior model. It is difficult to tell analytically why one method is better than the other. There are prior works related to Magnetic Resonance Imaging [23, 24, 25] where it was found that analysis prior yields better results.

2 Problem Formulation

A hyperspectral data cube of dimension $m \times n \times d$ having d spectral bands in it can be represented as $X = \begin{bmatrix} x_1 & x_2 & \dots & x_d \end{bmatrix}$ where each $x_i \in \mathbb{R}^{mn \times 1}$ is a spectral band obtained by vertical concatenation. Define $y = vec(Y)$ as vector representation of any 2D matrix obtained by vertical stacking of columns of matrix Y, and $Y = mat(y)$ as its reverse operation. We use small letters for vectors and capital letters for matrices. Using these notations, image acquisition model can be expressed as:

$$Y = X + N,$$

where X is original image, Y is noise corrupted image, and N is the noise.

The columns of X are images and hence have a sparse representation in transform domains like wavelet or finite difference. Since the images are spectrally correlated, the variation along the rows of X can be assumed to be smooth leading to a sparse representation in Fourier, wavelet or finite differencing. The spatio-spectral correlation can be jointly exploited by representing the datacube as a sparse signal: $Z = D_1 X D_2$. Here D_1, D_2 are sparsifying transforms along spatial and spectral dimensions respectively and Z denotes the sparse transform coefficients. Using this sparse signal representation, denoising problem can be framed as:

$$\min_Z \|Y - D_1^T Z D_2^T\|_1 + \lambda \|Z\|_1, \tag{3}$$

where λ is a regularization parameter. This is the general synthesis prior (GSP) formulation. For framing the analysis prior problem we model the images to be piecewise smooth and employ finite differencing to sparsify along the spatial dimension. Along the spectral dimension we employ an orthogonal sparsifying transform D. Using this, we get following general analysis prior (GAP) formulation:

$$\min_X \|Y - X\|_1 + \lambda \|D_h X D\|_1 + \lambda \|D_v X D\|_1, \tag{4}$$

where D_h, D_v are horizontal and vertical finite difference operators and λ is the regularization term.

For grayscale images having only one band the sparsifying transform along spectral dimension will not have any effect. In that case we get single band synthesis prior formulation of Eq. (1) as special case of (3) and TV denoising formulation in Eq. (2) as special case of (4). We are not aware of any efficient algorithm to solve such large scale problems. Therefore in the next section we derive algorithms for solving them.

3 Proposed Algorithms

3.1 General Synthesis Prior (GSP) Algorithm

We repeat GSP problem for the sake of convenience.

$$\min_Z \|Y - D_1^T Z D_2^T\|_1 + \lambda \|Z\|_1, \tag{5}$$

Since the variable Z is not separable therefore we substitute: $P = Y - D_1^T Z D_2^T$ and $Q = Z$ then (5) can be rewritten as constrained optimization problem:

$$\begin{aligned} \underset{Z}{\text{minimize}} \quad & \|P\|_1 + \lambda \|Q\|_1 \\ \text{subject to} \quad & P = Y - D_1^T Z D_2^T \\ & Q = Z \end{aligned}$$

The above constrained optimization problem can be expressed as unconstrained optimization problem using weak penalty function as follows:

$$\begin{aligned} \underset{Z,P,Q}{\text{minimize}} \; & \|P\|_1 + \lambda \|Q\|_1 + \mu_1 \|P - Y + D_1^T Z D_2^T\|_F^2 \\ & + \mu_2 \|Q - Z\|_F^2 \end{aligned}$$

where μ_1 and μ_2 are the regularization parameters and $\|\cdot\|_F$ represents Frobenius norm of a matrix. Since there are multiple regularization terms therefore split-Bregman [13] approach can be applied to solve this problem. Thus the above unconstrained problem can be expressed as:

$$\begin{aligned} \underset{Z,P,Q}{\text{minimize}} \; & \|P\|_1 + \lambda \|Q\|_1 + \mu_1 \|P - Y + D_1^T Z D_2^T - B_1^k\|_F^2 \\ & + \mu_2 \|Q - Z - B_2^k\|_F^2 \end{aligned}$$

where Bregman variables B_1 and B_2 are updated iteratively as follows:

$$\begin{aligned} B_1^{k+1} &= B_1^k + Y - P - D_1^T Z D_2^T \\ B_2^{k+1} &= B_2^k + Z - Q \end{aligned}$$

The above problem has three separable variables (Z, P, Q) and therefore we can split the problem in three simple subproblems. Let $A \otimes B$ denote the Kronecker product between matrices $A \in \mathbb{R}^{m \times n}$ and $B \in \mathbb{R}^{p \times q}$ defined as:

$$A \otimes B = \begin{bmatrix} a_{11}B & a_{12}B \dots & a_{1n}B \\ a_{21}B & a_{22}B \dots & a_{2n}B \\ \vdots & \vdots & \vdots \\ a_{m1}B & a_{m2}B \dots & a_{mn}B \end{bmatrix}_{mp \times nq}$$

Let $y_1 = vec(P - Y - B_1^k)$, $y_2 = vec(Q - B_2^k)$, $D = D_2 \otimes D_1^T$ then sub-problems can be expressed as follows:

$$\begin{aligned}
\text{P1}: &\quad \min_z \mu_1 \|y_1 + Dz\|_2^2 + \mu_2 \|y_2 - z\|_2^2 \\
\text{P2}: &\quad \min_p \|p\|_1 + \mu_1 \|p - y - b_1^k + Dz\|_2^2 \\
\text{P3}: &\quad \min_q \|q\|_1 + \mu_2 \|q - z - b_2^k\|_2^2.
\end{aligned}$$

Here we used the identity that $Y = AXB$ can be written as $y = (B^T \otimes A)x$. Above problem P1 is differentiable and convex whose solution we can obtain by solving

$$(\mu_1 D^T D + \mu_2 I)z = \mu_2 y_2 - \mu_1 D^T y_1,$$

iterativly using least square solvers. In case D_1 and D_2 are orthogonal transform we can simplify $D^T D$ as follows:

$$D^T D = (D_2^T \otimes D_1)(D_2 \otimes D_1^T) = D_2^T D_2 \otimes D_1 D_1^T = I,$$

which gives a closed form solution for problem P1 as:

$$z = \frac{\mu_2}{\mu_1 + \mu_2} y_2 - \frac{\mu_1}{\mu_1 + \mu_2} D^T y_1, \tag{6}$$

Problems P2 and P3 are ℓ_1-norm minimization problems in the following form:

$$\arg\min_x \|y - x\|_2^2 + \lambda \|x\|_1, \tag{7}$$

which can be solved by using soft-thresholding $\text{SoftTh}(y, \lambda)$ operation: $\hat{x} = \text{sign}(y) \times \max\left\{0, |y| - \frac{\lambda}{2}\right\}$. Algorithm 1 summaries the steps of the proposed GSP algorithm.

Algorithm 1 General Synthesis Prior (GSP) Algorithm

input: $D_1, D_2, D = D_2 \otimes D_1^T$, Y, λ, μ_1, μ_2, MaxIter.
output: $\hat{X}$, denoised image.
for $k = 1$ to MaxIter **do**
  $Z^{k+1} = mat(z^k)$ from (6)
  $P^{k+1} = \text{SoftTh}\left(Y + B_1^k - \text{mat}(Dz), \frac{1}{\mu_1}\right)$
  $Q^{k+1} = \text{SoftTh}\left(Z + B_2^k, \frac{\lambda}{\mu_2}\right)$
  $B_1^{k+1} = B_1^k - P^{k+1} + Y - D_1 Z^{k+1} D_2$
  $B_2^{k+1} = B_2^k + Z^{k+1} - Q^{k+1}$
end for
$\hat{X} = D_1^T Z^{k+1} D_2^T$

3.2 General Analysis Prior (GAP) Algorithm

We rewrite GAP formulation from previous section:

$$\arg\min_X \ \|Y - X\|_1 + \lambda \|D_h X D\|_1 + \lambda \|D_v X D\|_1 \tag{8}$$

As before recast (8) as follows:

$$\begin{aligned}
\underset{P,Q,R}{\text{minimize}} \quad & \|P\|_1 + \lambda \|Q\|_1 + \lambda \|R\|_1 \\
\text{subject to} \quad & P = Y - X \\
& Q = D_h X D \\
& R = D_v X D
\end{aligned}$$

which, using split-Bregman approach can be expressed as:

$$\begin{aligned}
\underset{X,P,Q,R,S}{\text{minimize}} \ & \|P\|_1 + \lambda \|Q\|_1 + \lambda \|R\|_1 + \mu_1 \|P - Y + X - B_1^k\|_F^2 \\
& + \mu_2 \|Q - D_h X D - B_2^k\|_F^2 + \mu_2 \|R - D_v X D - B_3^k\|_F^2
\end{aligned}$$

where Bregman variables are updated as :

$$\begin{aligned}
B_1^{k+1} &= B_1^k + Y - X - P \\
B_2^{k+1} &= B_2^k + D_h X D - Q \\
B_3^{k+1} &= B_3^k + D_v X D - R
\end{aligned}$$

Let $y_1 = vec(P - Y - B_1^k)$, $y_2 = vec(Q - B_2^k)$, $y_3 = vec(R - B_3^k)$, $W_h = D^T \otimes D_h$, $W_v = D^T \otimes D_v$, then above problem can be split into four separable problems as follows:

$$\begin{aligned}
\text{P4}: &\min_x \mu_1 \|y_1 + x\|_2^2 + \mu_2 \|y_2 - W_h x\|_2^2 + \mu_2 \|y_3 - W_v x\|_2^2 \\
\text{P5}: &\min_P \|P\|_1 + \mu_1 \|Y - X - P + B_1^k\|_F^2 \\
\text{P6}: &\min_Q \|Q\|_1 + \mu_2 \|Q - D_h X D - B_2^k\|_F^2 \\
\text{P7}: &\min_R \|R\|_1 + \mu_2 \|R - D_v X D - B_3^k\|_F^2
\end{aligned}$$

Problem P4 is differentiable and after simplification we get :

$$\left[\mu_1 I + \mu_2 W\right] x = \mu_2 (W_h^T y_2 + W_v^T y_3) - \mu_1 y_1 \tag{9}$$

where $W = (W_h^T W_h + W_v^T W_v)$, though finite difference operator is not orthogonal but corresponding matrices in (9) is very sparse because

$$W_h^T W_h = (D \otimes D_h^T)(D^T \otimes D_h) = I_d \otimes D_h^T D_h$$

and similarly $W_v^T W_v = I_d \otimes D_v^T D_v$ makes the system of equations in (9) large and sparse system therefore few iterations of iterative solver such as LSQR[26] will suffice to approximate x. Problems (P5), (P6) and (P7) can be solved using soft-thresholding as described in previously. Algorithm 2 summarizes the GAP algorithm.

Algorithm 2 General Analysis Prior (GAP) Algorithm

input: W_h, W_v, Y, λ, μ_1, μ_2, MaxIter.
output: $\hat{X}$: denoised image.
for $k = 1$ to MaxIter **do**
  $X^{k+1} = mat(\hat{x})$, solution from equation (9)
  $P^{k+1} = \text{SoftTh}\left(Y - X + B_1^k, \frac{1}{\mu_1}\right)$
  $Q^{k+1} = \text{SoftTh}\left(D_h X^{k+1} D + B_2^k, \frac{\lambda}{\mu_2}\right)$
  $R^{k+1} = \text{SoftTh}\left(D_v X^{k+1} D - B_3^k, \frac{\lambda}{\mu_2}\right)$
  $B_1^{k+1} = B_1^k + Y - P^{k+1} - X^{k+1}$
  $B_2^{k+1} = B_2^k + D_h X^{k+1} D - Q^{k+1}$
  $B_3^{k+1} = B_3^k + D_v X^{k+1} D - R^{k+1}$
end for
$\hat{X} = X^{k+1}$.

4 Experiments and Results

Two hyperspectral images were used for performing experiments. First image was of Reno city, NV, USA available

Table 1: PSNR (dB) values for Reno Image

Noise%	Noisy	MF	PSMF	IRN	SP	AP	GSP	GAP
Salt and Pepper Noise								
10	13.82	34.28	38.18	36.26	31.95	33.73	**42.34**	38.54
20	11.41	40.07	31.73	35.43	31.42	33.29	**41.07**	37.69
30	9.21	39.05	26.45	34.15	30.93	32.82	**39.82**	36.84
40	8.19	33.40	22.00	31.86	30.62	32.34	**38.46**	35.97
50	7.94	24.80	19.58	32.01	29.18	31.79	**36.73**	34.98
60	7.03	17.86	16.11	27.50	28.29	31.16	**35.12**	33.92
70	6.16	12.48	11.37	21.48	27.42	30.24	**33.41**	32.54
Random Valued Impulse Noise								
10	16.98	34.51	33.85	35.96	32.28	34.02	**42.82**	39.06
20	14.37	33.86	28.63	33.61	32.03	33.74	**41.84**	38.45
30	13.47	30.70	22.97	27.47	31.52	33.16	**40.10**	37.46
40	12.90	23.14	18.56	18.68	30.39	31.57	**37.03**	35.42
50	11.28	16.57	14.93	12.75	26.56	23.91	**29.94**	28.37
60	10.73	12.74	12.04	9.48	**15.44**	10.71	11.18	11.23
70	9.74	9.38	9.91	6.64	**12.06**	5.85	9.80	7.21

Table 2: PSNR(dB) values fro WDC image

Noise%	Noisy	MF	PSMF	IRN	SP	AP	GSP	GAP
Salt and Pepper Noise								
10	14.61	38.30	**48.03**	40.32	36.68	38.21	44.69	41.24
20	11.60	37.95	36.57	39.32	36.05	37.80	**43.68**	40.50
30	9.84	38.78	28.05	38.15	35.78	37.38	**42.62**	39.74
40	8.59	35.02	22.12	36.56	36.32	36.91	**41.21**	38.97
50	7.62	27.42	16.62	34.71	34.52	36.39	**40.12**	38.08
60	6.83	20.45	13.02	31.24	31.25	35.83	**38.49**	36.97
70	6.16	15.13	10.62	26.83	27.10	35.19	**35.69**	35.58
Random Valued Impulse Noise								
10	17.91	38.24	31.51	40.11	36.61	38.17	**44.56**	41.16
20	14.89	37.84	29.37	39.01	35.90	37.69	**43.46**	40.35
30	13.14	37.33	27.52	37.90	35.17	37.20	**42.14**	39.48
40	11.89	36.56	25.90	36.59	34.28	36.62	**40.57**	38.48
50	10.92	35.00	24.23	34.74	33.84	35.98	**38.78**	37.26
60	10.13	32.01	22.48	32.37	32.85	35.16	**36.77**	35.82
70	9.46	27.88	21.10	29.44	31.08	34.00	33.95	**34.24**

from [27]. This image is from High Resolution Imager (HRI) sensor having $2m$ spatial resolution and 5 nm band spacing covering spectral range of 395 to 2450 nm. Second image was of Washington DC mall available from [28]. This image is of Hyperspectral Digital Imagery Collection Experiment (HYDICE) sensor having $1m$ spatial resolution and 10-nm band spacing covering spectral range of 400 to 2500 nm. We used patchs of size $160 \times 160 \times 319$ from *Reno* image and $160 \times 160 \times 191$ from *WDC* image for experiments.

For GSP algorithm, orthogonal transform D_1 was selected as 2D Daubechies wavelet with filter length eight for spatial dimension. Along spectral dimension 1D Fourier transform was utilized as sparsifying basis in both GSP and GAP algorithms. We have empirically chosen the parameters required by our algorithm to yield good results for realistic noisy scenarios. Empirically best parameters for GSP algorithm were found to be $(\lambda, \mu_1, \mu_2, maxiter)$=$(2, 5, 5, 40)$ while for GAP best parameters were found to be $(\lambda, \mu_1, \mu_2, maxiter)$=$(2, 2, 2, 50)$. These parameters were tuned manually using cross validation. The tuning was performed so that the algorithms yield good results for a wide variety of noise levels. Our proposed technique is robust to large range of noise corruption (upto 50%). A window size of 5×5 was used with median filter. Since IRN algorithm converges in five loops as mentioned in [29] therefore five loops were used in all experiments.

When input image is of single band then GAP and GSP algorithms behave as AP and SP algorithms respectively. Experiments were performed with both salt and pepper noise as well as random valued impulse noise. Original hyperspectral images were corrupted by 10% to 70% noise to get noisy images which were then denoised using different algorithms. We selected median filtering based techniques as well as optimization based techniques to compare the proposed algorithms. In particular, median filter (MF), progressive switching median filter (PSMF) [30], and iterative re-weighted norm (IRN) [29] minimization algorithms were selected for comparison. We have also compared with SP and AP problems which are solved as special case of GSP and GAP algorithms. Since all these algorithms were developed for single band therefore each band was separately denoised by applying the algorithms iteratively.

Tables 1 shows experimental results on Reno image for both salt and pepper noise and random valued impulse noise while Table 2 shows experimental results for WDC image. PSNR(dB) was calculated for 10% to 70% noise levels on both Reno and WDC hyperspectral images. Column titled *Noisy* shows PSNR value between noisy and original image. Maximum PSNR value is bold faced. We notice that for WDC image at 10% noise level, PSMF algorithm gives best results for salt and pepper noise but PSNR decreases for all other noise levels. There is degradation in PSNR values for large noise levels (for 60% and more) for Reno image however this 60% and more impulse noise is an unlikely scenario to be encountered in practice. Notice that use of sparsifying basis for spectral dimension has increased PSNR values for both GSP and GAP algorithms compared to their sequential counterparts SP and AP algorithms.

Figure 2 shows qualitative visual comparison of reconstruction quality for 50% salt and pepper noise on $256 \times 256 \times 191$ patch of WDC image. Three bands(20, 80, and 170) are shown in false color with histogram equalization for better visual quality only. Median filtering and PSMF are not able to remove high noise in Fig. 2(c) and Fig. 2(d). IRN reduces noise but image details are not well preserved as shown in Fig. 2(e). SP algorithm also reduces noise but over-smooths the image and AP algorithm introduces some blurry effect in the image. Both GSP and GAP were able to reduce noise as well as preserve edge information compared to other algorithms. We notice that PSNR need not always be consistent with visual quality. Visual quality is a subjective evaluation and depends on the application-whether one wants denoised but smooth images or sharp but noisy ones. PSNR value is high if the image is non-noisy even if it is overtly smoothed (as in our case with synthesis prior Fig. 2(f)); the PSNR values are low for sharp but noise images, e.g. MF (Fig. 2(c)) and IRN (Fig. 2(e)).

Figures 3a and 3b shows the convergence plot for our GSP and GAP algorithms. The objective function does not decrease monotonically. But this is expected as our algorithm is based upon the Split Bregman approach. After 30 iterations objective functions of both the algorithms does not decrease significantly hence we can choose number of iterations to be 30 for experimental purpose.

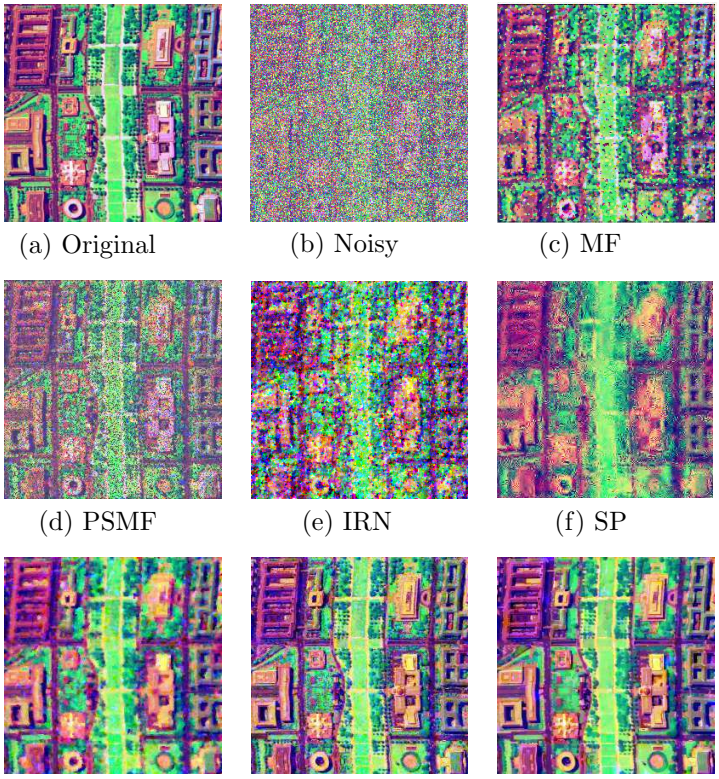

(a) Original (b) Noisy (c) MF

(d) PSMF (e) IRN (f) SP

(g) AP (h) GSP (i) GAP

Figure 2: Comparison of visual quality of denoising results for WDC image at 50% salt and pepper noise. Proposed GSP and GAP algorithms have better quality than other algorithms.

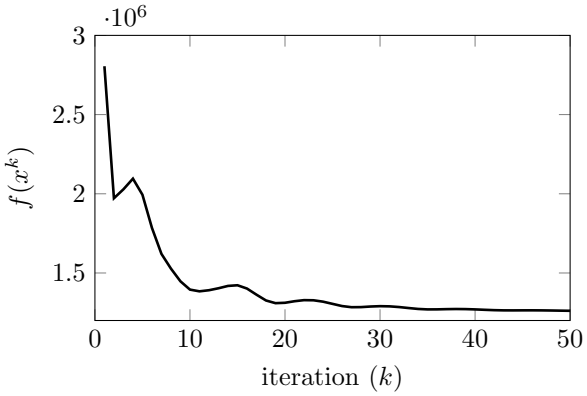

(a) GSP convergence

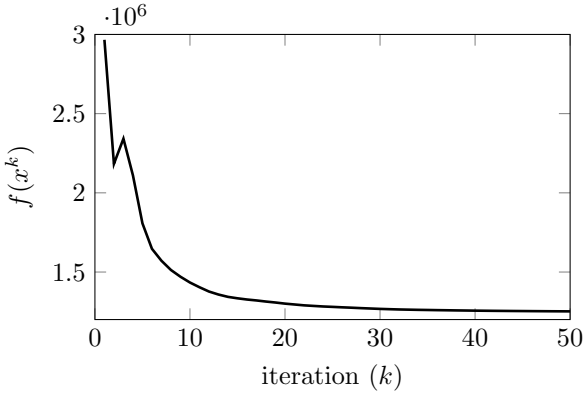

(b) GAP convergence

Figure 3: Convergence graphs for GSP and GAP algorithm for 50% salt and pepper noise on WDC image.

5 Conclusions

There have been studies to remove impulse noise from grayscale image and also Gaussian noise from hyperspectral images. In this work we addressed the problem of removing impulse noise from hyperspectral images by exploiting spatial redundancy and spectral correlation. We use two dictionaries to de-correlate hyperspectral datacube in both spatial and spectral dimensions which results in a very sparse representation. Our formulation leads to ℓ_1-norm regularized ℓ_1-norm data fidelity minimization problem. The problem has been formulated both as a synthesis prior and an analysis prior form.

Experiments were carried out on real hyperspectral datasets. Our technique was compared against recent denoising methods. For almost all cases (except when the image is corrupted by heavy noise $\sim 70\%$) our general synthesis prior technique yields best results.

Our Matlab implementation of both the algorithms are available at Matlab central [31] for the sake of reproducible research.

Acknowledgments

Hemant Kumar Aggarwal is supported by TCS research fellowship.

References

[1] Q. Yuan, L. Zhang, and H. Shen, "Hyperspectral Image Denoising Employing a Spectral-Spatial Adaptive Total Variation Model," *IEEE Trans. Geosci. Remote Sens.* **50**(10), 3660–3677 (2012).

[2] Q. Yuan, L. Zhang, and H. Shen, "Hyperspectral Image Denoising With a Spatial-Spectral View Fusion Strategy," *IEEE Trans. Geosci. Remote Sens.* **52**(5), 2314–2325 (2014).

[3] H. Zhang, W. He, L. Zhang, H. Shen, and Q. Yuan, "Hyperspectral Image Restoration Using Low-Rank Matrix Recovery," *IEEE Trans. Geosci. Remote Sens.* **52**(8), 4729–4743 (2014).

[4] Suwanee, "Dataset, last accessed : 14 Nov 2014." `http://www.spectir.com/free-data-samples/`.

[5] F. Chen, G. Ma, L. Lin, and Q. Qin, "Impulsive noise removal via sparse representation," *J. Electron. Imaging* **22**(4), 43014 (2013).

[6] L. Jin, H. Liu, X. Xu, and E. Song, "Quaternion-based color image filtering for impulsive noise suppression," *J. Electron. Imaging* **19**(4), 43003–43012 (2010).

[7] D. Baljozović, B. Kovačević, and A. Baljozović, "Novel method for removal of multichannel impulse noise based on half-space deepest location," *J. Electron. Imaging* **21**(1), 13025–13027 (2012).

[8] T. Mélange, M. Nachtegael, and E. E. Kerre, "Random impulse noise removal from image sequences based on fuzzy logic," *J. Electron. Imaging* **20**(1), 13016–13024 (2011).

[9] Y. Xia and M. S. Kamel, "Cooperative Recurrent Neural Networks for the Constrained L 1 Estimator," *IEEE Trans. Signal Process.* **55**(7), 3192–3206 (2007).

[10] J. Paredes and G. Arce, "Compressive sensing signal reconstruction by weighted median regression estimates," *IEEE Trans. Signal Process.* **59**(6), 2585–2601 (2011).

[11] H. Fu, M. K. Ng, M. Nikolova, and J. L. Barlow, "Efficient Minimization Methods of Mixed l2-l1 and l1-l1 Norms for Image Restoration," *SIAM J. Sci. Comput.* **27**, 1881–1902 (2006).

[12] L. I. Rudin, S. Osher, and E. Fatemi, "Nonlinear Total Variation Based Noise Removal Algorithms," *Phys. D Nonlinear Phenom.* **60**(1), 259–268 (1992).

[13] T. Goldstein and S. Osher, "The Split Bregman Method for L1-Regularized Problems," *SIAM J. Imaging Sci.* **2**, 323–343 (2009).

[14] Chunlin Wu, "Augmented Lagrangian Method for Total Variation Restoration with Non-Quadratic Fidelity," *Inverse Probl. Imaging* **5**(1), 237–261 (2011).

[15] Y. Shi and Q. Chang, "Efficient Algorithm for Isotropic and Anisotropic Total Variation Deblurring and Denoising," *J. Appl. Math.* **2013**, 1–14 (2013).

[16] J. Duran, B. Coll, and C. Sbert, "Chambolle's Projection Algorithm for Total Variation Denoising," *Impage Process. Line* **3**(2013), 311–331 (2013).

[17] P. Blomgren and T. F. Chan, "Color TV: total variation methods for restoration of vector-valued images.," *IEEE Trans. Image Process.* **7**, 304–9 (1998).

[18] L. Bar, A. Brook, N. Sochen, and N. Kiryati, "Deblurring of Color Images Corrupted by Impulsive Noise.," *IEEE Trans. Image Process.* **16**, 1101–11 (2007).

[19] A. Lam, I. Sato, and Y. Sato, "Denoising Hyperspectral Images Using Spectral Domain Statistics," in *Int. Conf. Pattern Recognit.*, 477–480 (2012).

[20] M. F. Duarte and R. G. Baraniuk, "Kronecker Compressive Sensing," *IEEE Trans. Image Process.* **21**(2), 494–504 (2012).

[21] M. F. Duarte and Y. C. Eldar, "Structured Compressed Sensing : From Theory to Applications," *IEEE Trans. Signal Process.* **59**(9), 4053–4085 (2011).

[22] W. Yin, S. Osher, D. Goldfarb, and J. Darbon, "Bregman Iterative Algorithms for L1-minimization with Applications to Compressed Sensing," *SIAM J. Imaging Sci.* **1**(1), 143–168 (2008).

[23] M. Lustig, D. Donoho, and J. M. Pauly, "Sparse mri: The application of compressed sensing for rapid mr imaging," *Magnetic resonance in medicine* **58**(6), 1182–1195 (2007).

[24] A. Majumdar and R. K. Ward, "On the Choice of Compressed Sensing Priors and Sparsifying Transforms for MR Image Reconstruction: An experimental study," *Signal Process. Image Commun.* **27**, 1035–1048 (2012).

[25] A. Majumdar and R. K. Ward, "Under-determined non-cartesian mr reconstruction with non-convex sparsity promoting analysis prior," in *Medical Image Computing and Computer-Assisted Intervention–MICCAI 2010*, 513–520, Springer (2010).

[26] M. A. Saunders, "Solution of Sparse Rectangular Systems Using LSQR and CRAIG," *BIT Numer. Math.* **35**(4), 588–604 (1995).

[27] Reno, "Dataset." `http://www.spectir.com/services/airborne-hyperspectral/`. Last accessed: 10th June 2014.

[28] WDC, "Dataset." `https://engineering.purdue.edu/%7ebiehl/MultiSpec/hyperspectral.html`. Last accessed: 10-June-2014.

[29] P. Rodríguez and B. Wohlberg, "Efficient minimization method for a generalized total variation functional," *IEEE Trans. Image Process.* **18**, 322–32 (2009).

[30] Z. Wang and D. Zhang, "Progessive Switching Median Filter for the Removal of Impulse Noise from Highly Corrupted Images," *IEEE Trans. Circuits Syst. Analog Digit. Signal Process.* **46**(1), 78–80 (1999).

[31] H. K. Aggarwal, "Matlab Implementation of Hyperspecttral Denoising Algorithms." `http://www.mathworks.in/matlabcentral/fileexchange/46988-hyperspectraldenoising-zip`. 2014.

Hemant Kumar Aggarwal is a PhD scholar at Indraprastha Institute of Information Technology since 2012. He received Masters' degree in computer science from Jawaharlal Nehru University, Delhi, India. He is recipient of TCS research fellowship. His research interests include multispectral and hyperspectral imaging, sparse recovery, and compressed sensing.

Angshul Majumdar is an assistant professor at Indraprastha Institute of Information Technology-Delhi from 2012. Prior to that he was associated with the Signal and Image Processing Lab at the University of British Columbia as a graduate student. He worked under the supervision of Dr. Rabab Ward. He is the author of more than 70 journal and conference papers. His research interests include compressed sensing and sparse recovery, low-rank matrix recovery, magnetic resonance imaging and color imaging.